

# Hybrid Functional and Plane Waves based *Ab Initio* Molecular Dynamics Study of the Aqueous $\text{Fe}^{2+}/\text{Fe}^{3+}$ Redox Reaction

Sagarmoy Mandal,<sup>[a,b,c]</sup> Ritama Kar,<sup>[a]</sup> Bernd Meyer,<sup>[b,c]</sup> Nisanth N. Nair\*<sup>[a]</sup>

Kohn-Sham density functional theory and plane wave basis set based *ab initio* molecular dynamics (AIMD) simulation is a powerful tool for studying complex reactions in solutions, such as electron transfer (ET) reactions involving  $\text{Fe}^{2+}/\text{Fe}^{3+}$  ions in water. In most cases, such simulations are performed using density functionals at the level of Generalized Gradient Approximation (GGA). The challenge in modelling ET reactions is the poor quality of GGA functionals in predicting properties of such open-shell systems due to the inevitable self-interaction error (SIE). While hybrid functionals can minimize SIE, AIMD at that level of theory is typically 150 times slower than GGA for systems containing  $\sim 100$  atoms. Among several approaches reported to speed-up AIMD simulations with hybrid functionals, the noise-stabilized MD (NSMD) procedure, together with the use of localized orbitals to compute the required exchange integrals, is an attractive option. In this work, we demonstrate the application of the NSMD approach for studying the  $\text{Fe}^{2+}/\text{Fe}^{3+}$  redox reaction in water. It is shown here that long AIMD trajectories at the level of hybrid density functionals can be obtained using this approach. Redox properties of the aqueous  $\text{Fe}^{2+}/\text{Fe}^{3+}$  system computed from these simulations are compared with the available experimental data for validation.

## Introduction

Electron transfer (ET) reactions are very important in many chemical and biological processes and are subjected to numerous experimental and theoretical investigations.<sup>[1]</sup> In this regard, aqueous ferrous-ferric ET has attracted many theoretical<sup>[2–18]</sup> studies as a prototype of more complex ET processes. In water solvent, both ferrous and ferric ions remain in stable hexaaqua complex form and build a well

defined solvent structure around them. Marcus has developed a very powerful theory<sup>[19–22]</sup> for describing the rate of ET from the electron donor to the electron acceptor in solution. The role of solvent polarization is very important in these ET events and the vertical energy gap was used as the reaction coordinate to estimate the redox potential and the rate of ET reactions. The reactant and product states involved in the ET process are described by two diabatic free energy surfaces. Using linear response theory, the free energy surfaces for the reactant and product states become parabolic functions of the vertical energy gap. Marcus theory has been successfully applied in many computational studies, and the linear response assumption was found to be valid.<sup>[23–27]</sup>

For applying simulation methods to model ET reactions in solution, Warshel and co-workers<sup>[28–31]</sup> have devised a strategy to use force field based classical molecular dynamics (MD) simulations. These statistical mechanics based theoretical results were fairly successful in predicting the experimentally observable redox properties. However, for a better understanding of the molecular level details of the solute-solvent structure, Kohn-Sham density functional theory (KS-DFT) based *ab initio* MD (AIMD) simulations are required. KS-DFT can give an accurate description of the solvent structure around the solute, leading to a better estimate of the vertical energy gap.<sup>[32]</sup> However, it is practically difficult to model the whole electron transfer process with KS-DFT due to the involved technical difficulties. In an attempt to avoid this problem, Sprik and co-workers<sup>[32–39]</sup> proposed to model only half reactions instead of the full reaction. It has been shown that the Marcus theory equally holds for half reactions and the results match well with experiments.

A redox property of interest within the Marcus theory is the reorganization free energy ( $\lambda$ ), which is defined as the free energy required to distort the ion from the most probable configuration of one state to the most probable configuration of the other state. Previous computational studies on the aqueous ferrous-ferric ET reaction reported  $\lambda$  as 3.6 eV<sup>[2]</sup> and 3.57 eV.<sup>[4]</sup> Experimental value of  $\lambda$  is 2.1 eV,<sup>[40]</sup> and thus these classical force field based calculations have overestimated the value of  $\lambda$ . One of the reasons for this discrepancy might be the lack of electronic polarization in the force field description of the solvent.<sup>[23]</sup> Thus, for a better quantitative result, KS-DFT based AIMD simulations are required, which can model the electronic polarizability of the solvent and the solute-solvent interaction more accurately. However, until now, these systems were described mostly with Generalized Gradient Approximation (GGA) functional based DFT simulations. Typically, GGA functional based AIMD simulations are inadequate in describing the electronic structure of open-shell systems, because

[a] Dr. S. Mandal, R. Kar, Prof. Dr. N. N. Nair\*  
Department of Chemistry, Indian Institute of Technology Kanpur (IITK), 208016 Kanpur, India  
E-mail: nnair@iitk.ac.in

[b] Dr. S. Mandal, Prof. Dr. B. Meyer  
Interdisciplinary Center for Molecular Materials and Computer Chemistry Center, Friedrich-Alexander-Universität Erlangen-Nürnberg (FAU), Nögelsbachstr. 25, 91052 Erlangen, Germany

[c] Dr. S. Mandal, Prof. Dr. B. Meyer  
Erlangen National High Performance Computing Center (NHR@FAU), Friedrich-Alexander-Universität Erlangen-Nürnberg, Martensstr. 1, 91058 Erlangen, Germany

they suffer from the self-interaction error (SIE).<sup>[41–44]</sup> Due to this error, these functionals tend to erroneously delocalize the excess electron over the donor and acceptor, and thus produce wrong estimates of vertical energy gaps, redox potentials and reorganization energies.<sup>[23,45–48]</sup> To address the problem of SIE, Marzari and co-workers formulated a penalty density-functional approach,<sup>[5]</sup> and applied it to study the aqueous ferrous-ferric ET reaction. The value of  $\lambda$  was found to be 2.0 eV in their study, which has excellent agreement with the experimental result. On the other hand, Sit and co-workers<sup>[17]</sup> have reported  $\lambda$  as 2.28 eV from a constrained DFT study, and Blumberger and co-workers<sup>[18]</sup> have found  $\lambda$  to be in the range of 1.70 - 1.95 eV from DFT/continuum calculations.

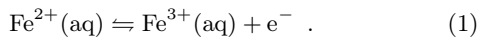
In our present work, we use hybrid functionals.<sup>[41,49–52]</sup> Hybrid functionals are known to reduce SIE and improve the quality of predicted redox properties.<sup>[45–48,53–59]</sup> However, hybrid functional based simulations are at least two orders of magnitude slower than the GGA functional based calculations.<sup>[60]</sup> Thus, AIMD simulations with hybrid functionals are rarely used<sup>[47,53]</sup> to study redox reactions. Recently, we have proposed a few methods to speed up hybrid functional and plane waves (PWs) based AIMD simulations.<sup>[61–65]</sup> These methods were successfully applied to model chemical reactions in explicit solvent. Here, we use one such method, namely the noise stabilized molecular dynamics (NSMD).<sup>[61]</sup> Our earlier implementation is modified to take care of spin polarised systems.

We model here the ferrous-ferric electron transfer process following the strategy of Sprik and co-workers. KS-DFT based AIMD simulations were performed to compute the redox potential and the solvent reorganization free energy. We benchmarked the performance of two different levels of density functionals, in particular, BLYP (GGA) and B3LYP (hybrid), for the prediction of redox properties. Additionally, for a fair comparison with the experimental results, we estimated the error due to finite size effect.

## Methods and Models

### Theory of Electron Transfer Reactions

This work focuses on the the following redox reaction



We follow the methodology that was introduced by Sprik and co-workers<sup>[32–39]</sup> employing DFT based AIMD simulations. In this approach, a half-cell redox reaction is considered and has been applied to various problems.<sup>[66–77]</sup> The central quantity of our interest is the vertical energy gap,  $\Delta E$ , defined as

$$\Delta E(\mathbf{R}) = E_{\text{Fe}^{3+}}(\mathbf{R}) - E_{\text{Fe}^{2+}}(\mathbf{R}) , \quad (2)$$

where  $E_M(\mathbf{R})$ ,  $M = \text{Fe}^{2+}$  or  $\text{Fe}^{3+}$ , is the ground state potential energies of the system in reduced and oxidized states for the given atomic configuration  $\mathbf{R}$ . Within the framework of Marcus theory,  $\Delta E$  can be used as the reaction coordinate to describe the free energy changes associated with the redox reaction.<sup>[28,29,78]</sup> Further, the probability distribution of the vertical energy gap  $\Delta E$ ,  $P_M(\Delta E)$ , is Gaussian shaped:

$$P_M(\Delta E) = \frac{1}{\sigma_{\Delta E}^M \sqrt{2\pi}} \exp \left[ -\frac{(\Delta E - \langle \Delta E \rangle_M)^2}{2(\sigma_{\Delta E}^M)^2} \right] . \quad (3)$$

Here,  $\langle \Delta E \rangle_M$  is the average of  $\Delta E$  and  $\sigma_{\Delta E}^M$  is the standard deviation of the distribution, for the redox state  $M$ . Now, the free energy surface for the system in state  $M$  can be constructed as a function of the energy gap as

$$F_M(\Delta E) = -k_B T \ln P_M(\Delta E) + \text{constant} , \quad (4)$$

where  $k_B$  and  $T$  are the Boltzmann constant and the temperature, respectively. The Gaussian shape of the probability distribution  $P_M(\Delta E)$  assures that the diabatic free energy plots for different oxidation states are parabolic, in accordance with Marcus theory.

If  $\Delta E_M^{\min}$  is the value of  $\Delta E$  for which  $F_M(\Delta E)$  is minimum, then the reorganization free energy for the system in the reduced state is given by

$$\lambda_{\text{Fe}^{2+}} = F_{\text{Fe}^{2+}}(\Delta E_{\text{Fe}^{3+}}^{\min}) - F_{\text{Fe}^{2+}}(\Delta E_{\text{Fe}^{2+}}^{\min}) \quad (5)$$

and for the oxidized state is

$$\lambda_{\text{Fe}^{3+}} = F_{\text{Fe}^{3+}}(\Delta E_{\text{Fe}^{2+}}^{\min}) - F_{\text{Fe}^{3+}}(\Delta E_{\text{Fe}^{3+}}^{\min}) . \quad (6)$$

The choice of  $\Delta E$  as the reaction coordinate leads to the following equation<sup>[28,78]</sup>

$$F_{\text{Fe}^{3+}}(\Delta E) - F_{\text{Fe}^{2+}}(\Delta E) = \Delta E , \quad (7)$$

which relates the free energy surfaces of both states. The free energy surface for the system in state  $\text{Fe}^{3+}$  (or  $\text{Fe}^{2+}$ ) can be computed by adding (or subtracting)  $\Delta E$  to (or from) the free energy surface of state  $\text{Fe}^{2+}$  (or  $\text{Fe}^{3+}$ ). On the other hand, under the linear response approximation,<sup>[71,76]</sup> we can compute the reorganization free energy as,

$$\lambda = (\langle \Delta E \rangle_{\text{Fe}^{2+}} - \langle \Delta E \rangle_{\text{Fe}^{3+}}) / 2 . \quad (8)$$

Further, the redox potential for the free energy change during the oxidation reaction can be computed as,

$$\Delta F = (\langle \Delta E \rangle_{\text{Fe}^{2+}} + \langle \Delta E \rangle_{\text{Fe}^{3+}}) / 2 , \quad (9)$$

Using Eqs. 8 and 9,  $\lambda$  and  $\Delta F$  can be computed from the ensemble average of  $\Delta E$  using AIMD simulations of the solvated  $\text{Fe}^{2+}$  and  $\text{Fe}^{3+}$  systems.

### Theory of Hybrid Functional based AIMD Simulations using NSMD

Hybrid functional based KS-DFT calculation requires the computation of the orbital-dependent Hartree-Fock (HF) exchange energy<sup>[49]</sup>

$$E_X^{\text{HF}} = - \sum_{i,j}^{N_{\text{orb}}} \langle \psi_i | v_{ij}(\mathbf{r}_1) | \psi_j \rangle , \quad (10)$$

with

$$v_{ij}(\mathbf{r}_1) = \left\langle \psi_j \left| \frac{1}{r_{12}} \right| \psi_i \right\rangle \quad (11)$$

and  $r_{12} = |\mathbf{r}_1 - \mathbf{r}_2|$ . For computational efficiency,  $v_{ij}(\mathbf{r})$  is often computed in reciprocal space (or G-space) using the fast Fourier transform algorithm.<sup>[60,79]</sup> If  $N_{\text{orb}}$  and  $N_G$  are the number of orbitals and the number of G-space grid points, respectively, the total computational cost for the HF exchange energy evaluation scales as  $N_{\text{orb}}^2 N_G \log N_G$ .<sup>[60]</sup> As a consequence, hybrid functional and PWs based AIMD simulations require very high computational time for typical systems of our interest containing few hundreds of atoms.

In the NSMD method,<sup>[61]</sup> we reduce the computational cost of HF exchange energy evaluation significantly by screening the KS orbital pairs in Eq. 10. In particular, we employ an unitary transformation based on the selected columns of the density matrix (SCDM) approach<sup>[80]</sup> to localize the KS orbitals in real space, as

$$|\phi_k\rangle = \sum_i^{N_{\text{orb}}} |\psi_i\rangle u_{ik}, \quad (12)$$

where  $u_{ik} \equiv (\mathbf{U})_{ik}$  and  $\mathbf{U}$  is the unitary matrix. Now,  $E_X^{\text{HF}}$  can be rewritten using the SCDM based localized orbitals as

$$E_X^{\text{HF}} = - \sum_{i,j}^{N_{\text{orb}}} \langle \phi_i | v_{ij}(\mathbf{r}_1) | \phi_j \rangle, \quad (13)$$

where  $v_{ij}(\mathbf{r})$  is computed as per Eq. (11) using  $\{\phi_i\}$ . For non-overlapping orbital pairs in real space,  $v_{ij}(\mathbf{r})$  will be zero and such pairs of orbitals will not contribute to the HF exchange energy. In our computations, we consider an orbital pair  $i$ - $j$  only if the criteria

$$\int d\mathbf{r} |\phi_i(\mathbf{r})\phi_j^*(\mathbf{r})| \geq \rho_{\text{cut}}$$

is satisfied. This screening procedure (based on a pair density cutoff  $\rho_{\text{cut}}$ ) allows for a substantial decrease in the number of orbital pairs entering in Eq. (13) during the HF exchange energy computation. The computational cost scales now as  $\tilde{N}_{\text{orb}}^2 N_G \log N_G$ , where  $\tilde{N}_{\text{orb}}$  is the effective number of orbital products considered in the calculation after screening, and in our case  $\tilde{N}_{\text{orb}} \ll N_{\text{orb}}$ .

However, during the molecular dynamics simulations, screening of orbital pairs based on  $\rho_{\text{cut}}$  introduce small errors in the wavefunctions and nuclear forces resulting in unstable dynamics with a drift in the total energy. To overcome this, following the work of Kühne *et al.*,<sup>[81]</sup> we employ the NSMD approach based on a noise stabilization of the dynamics by coupling a Langevin thermostat to the system.<sup>[61]</sup> In this case, the equations of motion for the ions can be written as

$$M_I \ddot{\mathbf{R}}_I = \mathbf{F}_I - \gamma \dot{\mathbf{R}}_I + \mathbf{x}_I, \quad I = 1, \dots, N, \quad (14)$$

where  $M_I$  is the ionic mass,  $\mathbf{F}_I$  is the ionic force, and  $\gamma$  is the friction coefficient of the Langevin thermostat.  $\mathbf{x}_I$  is the random noise that obeys the following expression:

$$\langle \mathbf{x}_I(0) \mathbf{x}_I(t) \rangle = 6\gamma M_I k_B T \Delta t, \quad (15)$$

where  $T$  and  $\Delta t$  are the target temperature of the system and the MD time step. The parameter  $\gamma$  is chosen in such a way that the correct average temperature is obtained, and the average of the total energy has no drift.

## Computational Details

We modelled a single  $\text{Fe}^{2+}$  or  $\text{Fe}^{3+}$  ion solvated in 64 water molecules inside a periodic simulation box of dimension  $12.414 \text{ \AA} \times 12.414 \text{ \AA} \times 12.414 \text{ \AA}$ , corresponding to a bulk water density of  $\sim 1.0 \text{ g cm}^{-3}$ . No counter ions were included in the system. Instead, a homogeneous positive background charge was added to maintain charge neutrality. In our calculations,  $\text{Fe}^{2+}$  and  $\text{Fe}^{3+}$  are considered in their high spin configurations. To simulate these open-shell systems, spin polarized periodic DFT calculations were performed. All computations were performed using a modified version of the CPMD program,<sup>[82,83]</sup> where we implemented the

NSMD approach.<sup>[61]</sup> We employed both BLYP<sup>[84,85]</sup> (GGA) and B3LYP<sup>[50]</sup> (hybrid) exchange correlation functionals together with norm-conserving Troullier-Martin type pseudopotentials.<sup>[86]</sup> The pseudopotential for iron includes the non-linear core correction.<sup>[87]</sup> The wavefunctions were expanded in a PW basis set with a cutoff of 90 Ry. Born-Oppenheimer molecular dynamics (BOMD) simulations were carried out in the canonical (NVT) ensemble at 300 K with a time step of 0.48 fs.

In the BLYP (GGA) functional based *NVT* ensemble simulations, the wavefunctions were optimized every MD step till the wavefunction gradient fell below  $10^{-6}$  a.u. A Nosé-Hoover chain thermostat<sup>[88]</sup> was used to control the temperature of the system at 300 K. The always stable predictor corrector (ASPC) extrapolation scheme<sup>[89]</sup> of order 5 was used to obtain the initial guess of wavefunctions. On the other hand, for all *NVT* MD simulations using the B3LYP (hybrid) functional, the wavefunctions were optimized till the magnitude of change in energy is below  $1 \times 10^{-3}$  a.u. Exchange integrals were calculated by the screened SCDM orbitals with a pair density cutoff of  $\rho_{\text{cut}} = 4 \times 10^{-3}$ . We employed the NSMD approach to perform BOMD simulations. The Langevin thermostat parameter, the friction coefficient  $\gamma$ , was set to  $1 \times 10^{-3} \text{ a.u.}^{-1}$ , and the target temperature  $T$  was set to 300 K. For the initial guess of the wavefunctions, the ASPC extrapolation scheme of order 2 was used.

For these systems, the hybrid calculations using NSMD could achieve a speed up of  $\sim 12$  times per MD step compared to the conventional hybrid density functional based AIMD simulation on 280 cores (14 nodes, each with two Intel Xeon E5-2630v4 Broadwell chips with 10 cores running at 2.2 GHz with 64 GB of RAM).

We performed 20 ps (10 ps) of equilibration for the B3LYP (BLYP) simulations. Subsequent to this,  $\sim 20$  ps long production simulations were carried out in all the cases. To calculate the vertical energy gap (Eq. 2), we sampled equidistant configurations from the trajectories with a time interval of 20 fs. In total, we took 1000 equally sampled configurations from each of the trajectories. For every configuration, single point energy calculations were performed for the reduced ( $\text{Fe}^{2+}$ ) and the oxidized ( $\text{Fe}^{3+}$ ) states.

Additionally, to estimate the finite size effects, we performed BLYP calculations with two larger unit cells: (a) one  $\text{Fe}^{2+}/\text{Fe}^{3+}$  ion solvated in 92 water molecules within a periodic cubic simulation box of side  $14.010 \text{ \AA}$ ; (b) one  $\text{Fe}^{2+}/\text{Fe}^{3+}$  ion solvated in 137 water molecules inside a periodic cubic simulation box of side  $16.000 \text{ \AA}$ . For these two systems, we performed 5 ps *NVT* equilibration and 7 ps *NVT* production runs. The vertical energy gap was calculated by taking 500 snapshots sampled every  $\sim 14.5$  fs.

## Results and Discussion

### Solvation Structure

First, we compare the solvation structure of the  $\text{Fe}^{2+/3+}$  ions with BLYP and B3LYP functionals. The radial pair distribution functions (RDFs) of the metal with oxygen and hydrogen were calculated from all the trajectories and are shown in Figure 1. In all cases, we observe two distinct solvation shells around the  $\text{Fe}^{2+/3+}$  ions. The first (second) peak of the  $\text{Fe}^{2+}$ -O distribution appears at 2.17 (4.29)  $\text{\AA}$  and 2.15 (4.35)  $\text{\AA}$  with BLYP and B3LYP functionals, respectively. In case of the  $\text{Fe}^{3+}$ -O distributions, the first and

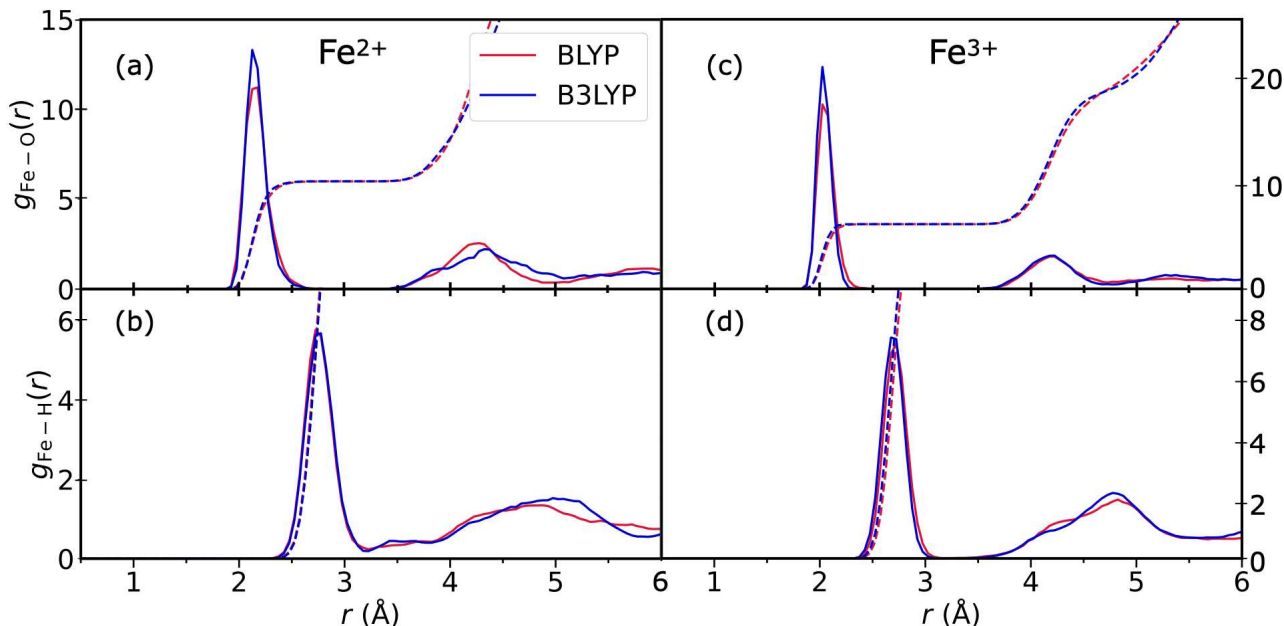


**Figure 1.** Comparison of (a)  $\text{Fe}^{2+}$ -O, (b)  $\text{Fe}^{2+}$ -H, (c)  $\text{Fe}^{3+}$ -O and (d)  $\text{Fe}^{3+}$ -H radial distribution functions (RDFs) for BLYP and B3LYP. The running integration number of the RDFs are also shown with dashed lines.

the second peaks appear at nearly the same location for both functionals. The first and the second peaks of the  $\text{Fe}^{2+}$ -H distributions are 0.02 Å and 0.18 Å shorter for BLYP compared to B3LYP. On the other hand, the locations of the first and second peaks in the  $\text{Fe}^{3+}$ -H distributions are not having much effect on the choice of the functional. These results are consistent with the previously reported computational<sup>[90–99]</sup> as well as experimental<sup>[100–103]</sup> data; see also Table 1.

In all cases, the RDFs are indicating a clear separation of the first and second solvation shell. During our simulations, we did not observe any exchange of water molecules between the first and second solvation shell. Due to the higher charge of the  $\text{Fe}^{3+}$  ion compared to its reduced form, we can notice that the first and the second peaks of the  $\text{Fe}^{3+}$ -O distributions are more sharply peaked as compared to the  $\text{Fe}^{2+}$  case.

Coordination numbers (CNs) of the ions with water molecules are computed by integrating RDFs; see Figure 2. The most preferred CN for both ions in water is 6.0 (see also Table 1), which is in agreement with earlier studies. We computed the CNs for the second solvation shell, and we find that our predicted second shell CN is larger than the experimental data, but close to some of the computational studies. The computed CN of the second shell for  $\text{Fe}^{2+}$  is higher as compared to that of  $\text{Fe}^{3+}$ . Interestingly, in the B3LYP simulations, we observe higher CN values for the second shell compared to BLYP, see Figure 2.

To further examine the geometry of the hexaaqua complex, we compare in Figure 3 the probability distribution of the cosine of O-Fe-O angle in the first solvation shell of the  $\text{Fe}^{2+/3+}$  ions from the BLYP and B3LYP functional based AIMD simulations. The distribution functions show two peaks at -1.0 and 0.0, indicating almost perfect octahedral arrangement of the water molecules. By comparing the average O-H bond distance and H-O-H angle of the water molecules in the first and the second coordination sphere, we conclude that the solvation structure is less affected by

the functionals, see Table 1.

## Electron Transfer Reaction

We then computed the redox properties of the aqueous  $\text{Fe}^{2+}$  and  $\text{Fe}^{3+}$  systems. The vertical energy gap (Eq. 2) is calculated for the structures sampled during the MD simulations. Redox properties were calculated from the fluctuation of  $\Delta E$  and are reported in Table 2.  $\langle \Delta E \rangle_{\text{Fe}^{2+}}$ , computed from BLYP and B3LYP simulations, are almost identical. However,  $\langle \Delta E \rangle_{\text{Fe}^{3+}}$  from the BLYP run is 0.46 eV larger than for B3LYP. Nearly identical values of  $\sigma_{\Delta E}^{\text{Fe}^{2+}}$  and  $\sigma_{\Delta E}^{\text{Fe}^{3+}}$  show the validity of the linear response assumption underlying the Marcus theory. The standard deviations of  $\Delta E$  are higher in B3LYP cases as compared to BLYP, implying a much larger spread in the  $\Delta E$  values during the hybrid functional based simulations.

In Figure 5, we show the probability distributions of  $\Delta E$ . Gaussian functions are used to fit these probability distributions within the range  $[\langle \Delta E \rangle_M - 2\sigma_{\Delta E}^M, \langle \Delta E \rangle_M + 2\sigma_{\Delta E}^M]$ . The  $R^2$  values of these fits are 0.973, 0.952, 0.996 and 0.962 for the  $\text{Fe}^{2+}$  (BLYP),  $\text{Fe}^{2+}$  (B3LYP),  $\text{Fe}^{3+}$  (BLYP) and  $\text{Fe}^{3+}$  (B3LYP) systems, respectively. We notice a broader distribution in case of B3LYP results as compared to BLYP, in accordance to the values of the standard deviations we computed earlier. The consequence of this observation in the curvature of the free energy profiles will be discussed shortly. Free energy surfaces are reconstructed from the probability distributions (using Eq. 4), see Figure 6. We have aligned the minima of all free energy curves to zero. For the region far from equilibrium, we used the linear free energy relation of Eq. 7 to obtain the data points. Free energy data were then fitted with parabolic functions, and the  $R^2$  values for the fits are 0.9995, 0.9998, 0.9995 and 0.9998 for the  $\text{Fe}^{2+}$  (BLYP),  $\text{Fe}^{2+}$  (B3LYP),  $\text{Fe}^{3+}$  (BLYP) and  $\text{Fe}^{3+}$  (B3LYP) cases, respectively. This result suggests that the aqueous  $\text{Fe}^{2+/3+}$  redox system behaves linearly with respect to the solvent response, as reported in earlier studies.<sup>[2,5–7]</sup>

**Table 1..** Comparison of structural properties of the first and second solvation shell (SS) of water around  $\text{Fe}^{2+}$  and  $\text{Fe}^{3+}$  ions in our simulations with other data from simulations (Sim.) and experimental (Expt.) studies.

SS	Property	$\text{Fe}^{2+}$				$\text{Fe}^{3+}$			
		BLYP	B3LYP	Sim. <sup>[a]</sup>	Expt. <sup>[b]</sup>	BLYP	B3LYP	Sim. <sup>[a]</sup>	Expt. <sup>[b]</sup>
1st	$r_{\text{Fe-O}}^{\text{max}}$ (Å)	2.17	2.15	2.09 – 2.13	2.10 – 2.28	2.04	2.03	1.96 – 2.10	1.98 – 2.05
	$r_{\text{Fe-H}}^{\text{max}}$ (Å)	2.73	2.75	2.40 – 2.76		2.71	2.70	2.66 – 2.77	
	CN	6.0	6.0	6.0	6.0	6.0	6.0	6.0	6.0
	$r_{\text{O-H}}$ (Å)	0.99	0.98	1.03		1.0	1.0	1.01 – 1.06	
	$\theta_{\text{H-O-H}}$ (°)	106.2	106.3	102.0		107.1	107.1	98.8 – 107.0	
2nd	$r_{\text{Fe-O}}^{\text{max}}$ (Å)	4.29	4.35	4.25 – 4.50	4.30 – 4.51	4.20	4.20	4.11 – 4.30	4.09 – 4.80
	$r_{\text{Fe-H}}^{\text{max}}$ (Å)	4.81	4.99			4.81	4.77	4.76 – 4.96	
	CN	13.0	15.3	11.6 – 14.4	12	12.2	12.6	11.0 – 14.0	12
	$r_{\text{O-H}}$ (Å)	0.99	0.98	1.02		0.99	0.98	1.02	
	$\theta_{\text{H-O-H}}$ (°)	106.4	107.0	104.7		106.7	105.9	104.4	

[a] Refs. 90–99. [b] Refs. 100–103.

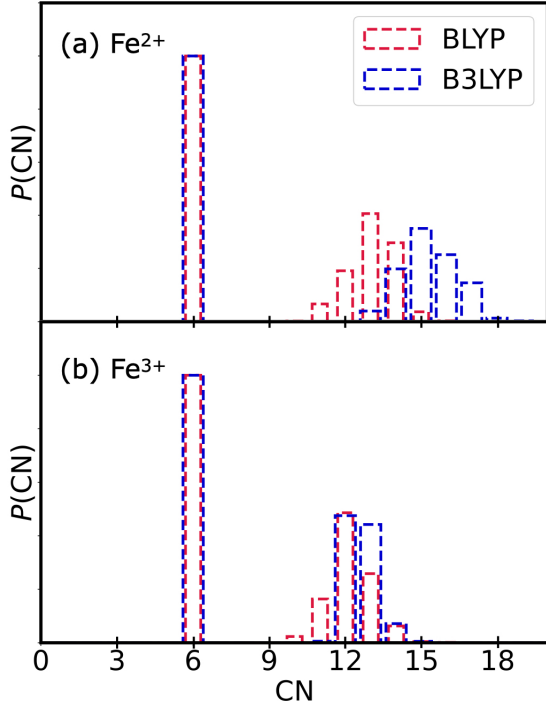


**Figure 2..** Coordination number (CN) distribution in the first and second solvation shells of (a)  $\text{Fe}^{2+}$  and (b)  $\text{Fe}^{3+}$  ions.

Interestingly, the curvature and the location of the minima in the free energy profiles differ for the two functionals.

Finally, the solvent reorganization free energies were calculated from the fitted parabolic curves (Eqs. 5 and 6) and from the vertical energy data (Eq. 8). We find that the computed reorganization energies agree well with each other. This further validates the linear response assumption of Marcus theory. We find that the B3LYP functional based calculations predict a higher  $\lambda$  value (1.10 eV) compared to GGA (0.88 eV). Also, we find that the calculated redox potential is 0.50 eV and 0.26 eV for BLYP and B3LYP cases, respectively.

Before comparing our results with the experimental estimates, we need to account for the errors due to the fi-

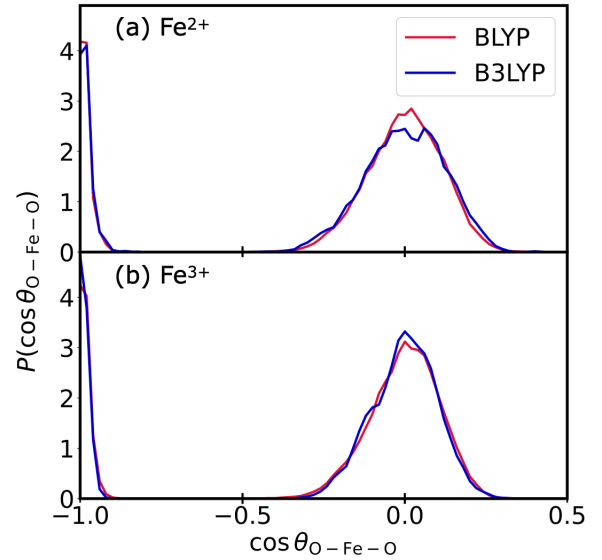


**Figure 3..** Comparison of the probability distribution of the cosine of O-Fe-O angle in the first solvation shell of (a)  $\text{Fe}^{2+}$  and (b)  $\text{Fe}^{3+}$  ions.

nite size effect. It has been reported that the finite size effect<sup>[66,68,69,104,105]</sup> contributes substantially to the reorganization free energy. Generally, the error in  $\lambda$  is inversely proportional to the side length of the box and is found to be as large as an eV or more.<sup>[66,68]</sup> Sprik and co-workers<sup>[68]</sup> have concluded that  $\lambda$  is usually underestimated. These authors have shown that correction for the solvent reorganization energy is

$$\lambda_C = -\frac{\Delta q^2}{2L} \xi_{\text{EW}} \left( \frac{1}{\epsilon_{\text{op}}} - \frac{1}{\epsilon_{\text{st}}} \right), \quad (16)$$

where  $L$ ,  $\Delta q$  and  $\xi_{\text{EW}}$  are the length of the periodic simulation cell, change in charge during the oxidation reaction and the Madelung constant ( $\xi_{\text{EW}} = -2.837297$  for a cubic unit cell), respectively. Here,  $\epsilon_{\text{op}} = 1.78$ ,  $\epsilon_{\text{st}} = 78.4$  are the optical and static dielectric constant, respectively.<sup>[106,107]</sup> Using this,  $\lambda_C$  for the 64 water system was found to be about 0.91 eV.

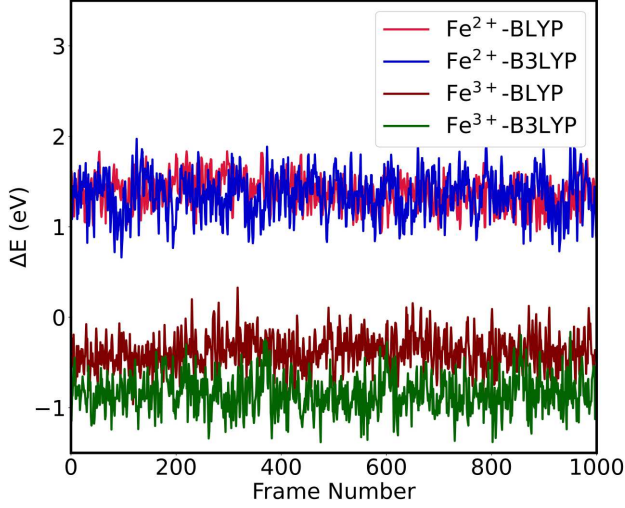


**Figure 4..** Vertical energy gap ( $\Delta E$ ) during BLYP and B3LYP simulations of  $\text{Fe}^{2+}$  and  $\text{Fe}^{3+}$  systems.

**Table 2..** Redox properties computed from the AIMD simulation of the aqueous  $\text{Fe}^{2+}$  and  $\text{Fe}^{3+}$  systems.

Properties	BLYP (eV)	B3LYP (eV)
$\langle \Delta E \rangle_{\text{Fe}^{2+}}$	$1.38 \pm 0.03$	$1.35 \pm 0.02$
$\langle \Delta E \rangle_{\text{Fe}^{3+}}$	$-0.38 \pm 0.02$	$-0.84 \pm 0.02$
$\sigma_{\Delta E}^{\text{Fe}^{2+}}$	0.17	0.23
$\sigma_{\Delta E}^{\text{Fe}^{3+}}$	0.19	0.20
$\lambda_{\text{Fe}^{2+}}$	0.87	1.07
$\lambda_{\text{Fe}^{3+}}$	0.87	1.07
$\lambda$	$0.88 \pm 0.02$	$1.10 \pm 0.01$
$\Delta F$	$0.50 \pm 0.02$	$0.26 \pm 0.01$

In an alternative approach, one performs a series of simulations with increasing system size, and  $\lambda$  is computed for different system sizes, in particular, different simulation box lengths  $L$ .  $\lambda$  is then plotted versus  $1/L$  and the extrapolated linear fit to  $1/L \rightarrow 0$  gives the value of  $\lambda$  at infinite dilution. Blumberger and co-workers<sup>[66]</sup> have shown that such a linear fit with  $1/L$  can underestimate the finite size correction. As a better alternative, they proposed to fit using  $(1/L)^{1/2}$ . To measure the finite size effects of our results using this approach, we carried out two additional simulations with bigger unit cells as discussed in the Methods and Models section. In Table 3, we presented our results for these two systems with 92 and 137 water molecules at the level of BLYP functionals. Together with the data from the 64 water simulation, we plot the reorganization free energy ( $\lambda$ ) as a function of  $(1/L)^{1/2}$  (Figure 7). We used linear regression to fit these data points with a straight line. The  $R^2$  value of our fit is 0.936, which is reasonable, considering the few data points considered here. By extrapolating to the infinite dilution limit, we found that the value of  $\lambda$  at infinite dilution is 1.84 eV. Thus, in the computed  $\lambda$  values with 64 water molecules, we have added the correction term of 0.96 eV. The corrected results are in good agreement with the value of  $\lambda_C = 0.91$  eV computed with Eq. 16. With this correction, our estimates of  $\lambda$  are 1.84 eV and 2.06 eV for BLYP (GGA) and B3LYP (hybrid) based simulations.

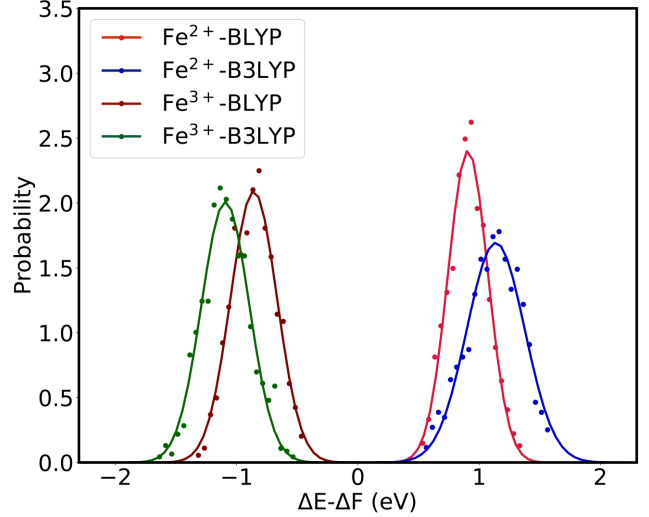


**Figure 5..** Probability distribution of  $\Delta E$  for the aqueous  $\text{Fe}^{2+}$  and  $\text{Fe}^{3+}$  systems. The gap energies are shifted by  $\Delta F$  (Eq. 9). Probability distributions are fitted with Gaussian functions (solid lines).

**Table 3..** Redox properties computed from the AIMD simulation of larger aqueous  $\text{Fe}^{2+/3+}$  systems using BLYP density functional.

Properties	System 1	System 2
$N_{\text{water}}^{\text{[a]}}$	92	137
$L$ (Å) <sup>[b]</sup>	14.01	16.00
$\langle \Delta E \rangle_{\text{Fe}^{2+}}$ (eV)	$1.50 \pm 0.03$	$1.52 \pm 0.02$
$\langle \Delta E \rangle_{\text{Fe}^{3+}}$ (eV)	$-0.43 \pm 0.02$	$-0.47 \pm 0.02$
$\sigma_{\Delta E}^{\text{Fe}^{2+}}$ (eV)	0.18	0.16
$\sigma_{\Delta E}^{\text{Fe}^{3+}}$ (eV)	0.20	0.20
$\lambda$ (eV)	$0.96 \pm 0.02$	$0.99 \pm 0.01$
$\Delta F$ (eV)	$0.53 \pm 0.02$	$0.52 \pm 0.01$

[a] Number of water molecules present in the system. [b] Box length of the simulation cell.

The experimental value of  $\lambda$  for this redox reaction is 2.1 eV.<sup>[40]</sup> Thus, our hybrid functional based prediction of  $\lambda$  is in excellent agreement with the experimental result.

Comparison of the computed redox potential  $\Delta F$  with the experimental result is also not straightforward. First, finite size correction has to be applied and the same experimentally considered zero electrostatic potential reference has to be used in computations.<sup>[66]</sup> The finite size correction for  $\Delta F$  is often evaluated by a linear fit of  $\Delta F$  with  $(1/L)^3$ .<sup>[66,68]</sup> Then, the extrapolated linear fit can be used to obtain the value of  $\Delta F$  at the infinite dilution limit. However, our results suggest that the change in  $\Delta F$  is minimal with the system size (see Tables 2 and 3). Thus, we refrain from computing the finite size correction for  $\Delta F$ . Additionally, it is not trivial to compute the difference in the absolute electrostatic potential reference between our periodic DFT calculation and the experiment. Hence, we could not compare the computed redox potential directly with the experimental results. Regardless of the corrections, we observe that the value of  $\Delta F$  for the BLYP case is 0.24 eV larger than for B3LYP, and that highlights the effect of the functional.



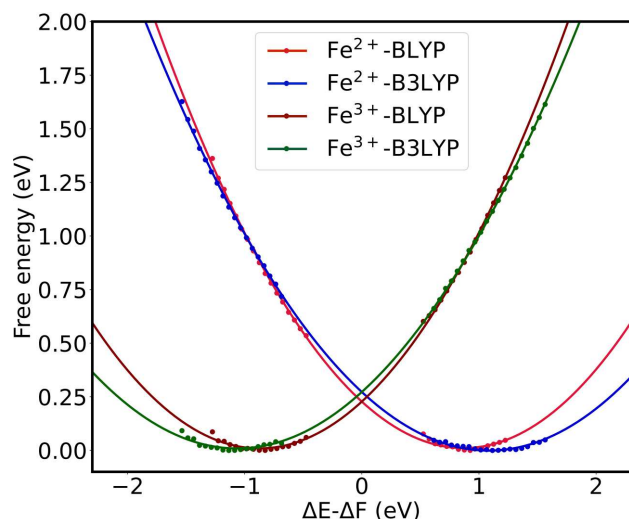


**Figure 6..** Free energy profiles as a function of  $\Delta E$  for the aqueous  $\text{Fe}^{2+}$  and  $\text{Fe}^{3+}$  systems. Free energy curves are fitted with parabolic functions (solid lines).

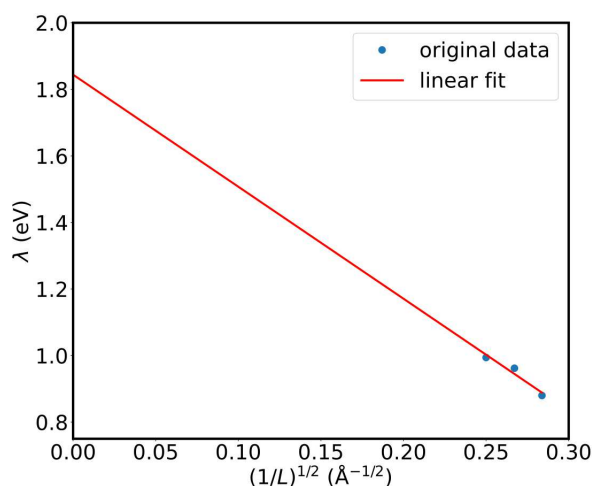


**Figure 7..** Linear fit of the reorganization free energy ( $\lambda$ ) with  $(1/L)^{1/2}$ .

## Conclusion

In this work, we studied the aqueous  $\text{Fe}^{2+}/\text{Fe}^{3+}$  redox system employing the KS-DFT based AIMD technique. Due to the SIE, GGA functionals are known to introduce errors in the redox properties of such open-shell systems. Hybrid functional based AIMD simulations are better for such studies, as SIE is minimized because of the inclusion of some percentage of HF exchange. However, hybrid functional based AIMD simulations with PW basis set are rarely performed due to the computational cost involved. To overcome this, we performed NSMD based AIMD simulations wherein the HF exchange was computed using screened SCDM-based localized orbitals. With this approach, we are able to generate long AIMD trajectories of aqueous  $\text{Fe}^{2+}/\text{Fe}^{3+}$  redox systems containing  $\sim 200$  atoms.

Using our simulation results, we compared the accuracy of BLYP (GGA) and B3LYP (hybrid) functionals for studying this reaction. Although we observed negligible differences in the first solvation shell structure of the ions, the second

solvation shell structure showed prominent differences. To compute the redox properties, we followed the half-cell reaction modelling strategy by Sprik and co-workers employing AIMD simulations. Specifically, we computed the redox potential and the solvent reorganization free energy ( $\lambda$ ) using the vertical gap energy as the reaction coordinate to model the  $\text{Fe}^{2+}/\text{Fe}^{3+}$  redox reaction.

We found that the free energy curves for the reduced and oxidized state of the system can be well approximated by two parabolas with the same curvature in accordance to the linear response assumption of Marcus theory. The BLYP GGA functional predicted a 0.22 eV lower solvent reorganization energy ( $\lambda$ ) than the B3LYP hybrid functional. However, both functionals underestimate the solvent reorganization energy by  $\sim 1$  eV as compared to the experimental observations. Following the earlier reports, we computed the finite size corrections. After including this correction, amounting to 0.96 eV, the computed value of  $\lambda$  at the level of the hybrid functionals agrees well with the experimental data. These results demonstrate the importance of using hybrid functional based AIMD for the accurate prediction of redox properties in open-shell systems.

The work also shows that the NSMD technique along with screened localized orbitals is a good approach for speeding up hybrid density functional based AIMD simulations of complex chemical reactions in water. The protocols used here can also be used for studying other electron transfer reactions.

## Acknowledgements

The support and the resources provided by the Centre for Development of Advanced Computing (C-DAC), the National Supercomputing Mission (NSM), Government of India, the Science and Engineering Research Board (India) under the MATRICS (Ref. No. MTR/2019/000359), the German Research Foundation (DFG) through SFB 953 (project number 182849149), the Federal Ministry of Education and Research (BMBF), the state of Bavaria as part of the NHR Program, the Cluster of Excellence "Engineering of Advanced Materials" (EAM) and the "Competence Unit for Scientific Computing" (CSC) at the University of Erlangen-Nürnberg (FAU) are gratefully acknowledged. RK thanks the Council of Scientific & Industrial Research (CSIR), India, for her PhD fellowship. Computational resources were provided by the HPC facility (HPC2013) at IITK, the Erlangen Regional Computing Center (RRZE) at FAU, SuperMUC-NG (project pn98fa) at Leibniz Supercomputing Centre (LRZ) and PARAM Sanganak supercomputing facility under NSM at IITK.

## Conflict of Interest

The authors declare no conflict of interest.

**Keywords:** Electron transfer • Hybrid functionals • Marcus theory • Redox reaction • Reorganization free energy

## References

- [1] M. Bixon, J. Jortner, *Electron Transfer—from Isolated Molecules to Biomolecules*. In *Adv. Chem. Phys.*, pages 35–202, John Wiley & Sons, Ltd **1999**.
- [2] R. A. Kuharski, J. S. Bader, D. Chandler, M. Sprik, M. L. Klein, R. W. Impey, *J. Chem. Phys.* **1988**, *89*, 3248.
- [3] J. S. Bader, R. A. Kuharski, D. Chandler, *J. Chem. Phys.* **1990**, *93*, 230.
- [4] K. Ando, *J. Chem. Phys.* **2001**, *114*, 9470.
- [5] P. H.-L. Sit, M. Cococcioni, N. Marzari, *Phys. Rev. Lett.* **2006**, *97*, 028303.
- [6] C. Drechsel-Grau, M. Sprik, *J. Chem. Phys.* **2012**, *136*, 034506.
- [7] C. Drechsel-Grau, M. Sprik, *Molecular Physics* **2015**, *113*, 2463.
- [8] A. Bouzid, A. Pasquarello, *J. Chem. Theory Comput.* **2017**, *13*, 1769.
- [9] X. Zeng, H. Hu, X. Hu, A. J. Cohen, W. Yang, *J. Chem. Phys.* **2008**, *128*, 124510.
- [10] A. Migliore, P. H.-L. Sit, M. L. Klein, *J. Chem. Theory Comput.* **2009**, *5*, 307.
- [11] D. A. Rose, I. Benjamin, *J. Chem. Phys.* **1994**, *100*, 3545.
- [12] D. A. Rose, I. Benjamin, *Chem. Phys. Lett.* **1995**, *234*, 209.
- [13] R. B. Yelle, T. Ichiye, *J. Phys. Chem. B* **1997**, *101*, 4127.
- [14] J. B. Straus, A. Calhoun, G. A. Voth, *J. Chem. Phys.* **1995**, *102*, 529.
- [15] A. Calhoun, G. A. Voth, *J. Phys. Chem. B* **1998**, *102*, 8563.
- [16] J. Li, C. L. Fisher, J. L. Chen, D. Bashford, L. Noodleman, *Inorg. Chem.* **1996**, *35*, 4694.
- [17] C. Ku, P. H.-L. Sit, *J. Chem. Theory Comput.* **2019**, *15*, 4781.
- [18] R. Seidel, S. Thürmer, J. Moens, P. Geerlings, J. Blumberger, B. Winter, *J. Phys. Chem. B* **2011**, *115*, 11671.
- [19] R. A. Marcus, *J. Chem. Phys.* **1956**, *24*, 966.
- [20] R. A. Marcus, *J. Chem. Phys.* **1957**, *26*, 867.
- [21] R. A. Marcus, *J. Chem. Phys.* **1965**, *43*, 679.
- [22] R. A. Marcus, *Rev. Mod. Phys.* **1993**, *65*, 599.
- [23] J. Blumberger, *Phys. Chem. Chem. Phys.* **2008**, *10*, 5651.
- [24] J. Blumberger, *Chem. Rev.* **2015**, *115*, 11191.
- [25] R. Marcus, N. Sutin, *Biochim. Biophys. Acta - Rev. Bioenerg.* **1985**, *811*, 265.
- [26] R. A. Marcus, *Annu. Rev. Phys. Chem.* **1964**, *15*, 155.
- [27] B. S. Brunschwig, N. Sutin, *Coord. Chem. Rev.* **1999**, *187*, 233.
- [28] A. Warshel, *J. Phys. Chem.* **1982**, *86*, 2218.
- [29] G. King, A. Warshel, *J. Chem. Phys.* **1990**, *93*, 8682.
- [30] A. Warshel, J. Hwang, *J. Chem. Phys.* **1986**, *84*, 4938.
- [31] J. K. Hwang, A. Warshel, *J. Am. Chem. Soc.* **1987**, *109*, 715.
- [32] J. Blumberger, M. Sprik, *Theor. Chem. Acc.* **2006**, *115*, 113.
- [33] J. Blumberger, I. Tavernelli, M. L. Klein, M. Sprik, *J. Chem. Phys.* **2006**, *124*, 064507.
- [34] J. Blumberger, M. Sprik, *J. Phys. Chem. B* **2004**, *108*, 6529.
- [35] J. Blumberger, L. Bernasconi, I. Tavernelli, R. Vuilleumier, M. Sprik, *J. Am. Chem. Soc.* **2004**, *126*, 3928.
- [36] J. VandeVondele, M. Sulpizi, M. Sprik, *Angew. Chem. Int. Ed.* **2006**, *45*, 1936.
- [37] J. Blumberger, M. Sprik, *J. Phys. Chem. B* **2005**, *109*, 6793.
- [38] J. VandeVondele, R. Lynden-Bell, E. J. Meijer, M. Sprik, *J. Phys. Chem. B* **2006**, *110*, 3614.
- [39] F. Costanzo, M. Sulpizi, R. G. D. Valle, M. Sprik, *J. Chem. Phys.* **2011**, *134*, 244508.
- [40] K. M. Rosso, J. R. Rustad, *J. Phys. Chem. A* **2000**, *104*, 6718.
- [41] W. Koch, M. C. Holthausen, *A Chemist's Guide to Density Functional Theory*, WILEY-VCH, New York **2001**.
- [42] A. J. Cohen, P. Mori-Sánchez, W. Yang, *Science* **2008**, *321*, 792.
- [43] J. P. Perdew, A. Zunger, *Phys. Rev. B* **1981**, *23*, 5048.
- [44] P. Mori-Sánchez, A. J. Cohen, W. Yang, *Phys. Rev. Lett.* **2008**, *100*, 146401.
- [45] F. H. Hodel, S. Lubner, *J. Chem. Theory Comput.* **2017**, *13*, 974.
- [46] C. Adriaanse, J. Cheng, V. Chau, M. Sulpizi, J. VandeVondele, M. Sprik, *J. Phys. Chem. Lett.* **2012**, *3*, 3411.
- [47] L.-P. Wang, T. Van Voorhis, *J. Chem. Theory Comput.* **2012**, *8*, 610.
- [48] J. Cheng, X. Liu, J. VandeVondele, M. Sulpizi, M. Sprik, *Acc. Chem. Res.* **2014**, *47*, 3522.
- [49] R. M. Martin, *Electronic Structure: Basic Theory and Practical Methods*, Cambridge University Press, Cambridge **2004**.
- [50] A. D. Becke, *J. Chem. Phys.* **1993**, *98*, 5648.
- [51] J. P. Perdew, M. Ernzerhof, K. Burke, *J. Chem. Phys.* **1996**, *105*, 9982.
- [52] J. Heyd, G. E. Scuseria, M. Ernzerhof, *J. Chem. Phys.* **2003**, *118*, 8207.
- [53] C. S. Ahart, K. M. Rosso, J. Blumberger, *J. Chem. Theory Comput.* **2022**, *18*, 4438.
- [54] B. Rudshteyn, J. L. Weber, D. Coskun, P. A. Devlaminck, S. Zhang, D. R. Reichman, J. Shee, R. A. Friesner, *J. Chem. Theory Comput.* **2022**, *18*, 2845.
- [55] S. Niu, T. Ichiye, *Mol. Simul.* **2011**, *37*, 572.
- [56] J. Calvo-Castro, C. J. McHugh, A. J. McLean, *Dyes Pigm.* **2015**, *113*, 609.
- [57] H. Oberhofer, J. Blumberger, *J. Chem. Phys.* **2010**, *133*, 244105.
- [58] M. T. Nielsen, K. A. Moltved, K. P. Kepp, *Inorg. Chem.* **2018**, *57*, 7914.
- [59] D. Yepes, R. Seidel, B. Winter, J. Blumberger, P. Jaque, *J. Phys. Chem. B* **2014**, *118*, 6850.
- [60] S. Chawla, G. A. Voth, *J. Chem. Phys.* **1998**, *108*, 4697.
- [61] S. Mandal, J. Debnath, B. Meyer, N. N. Nair, *J. Chem. Phys.* **2018**, *149*, 144113.
- [62] S. Mandal, N. N. Nair, *J. Chem. Phys.* **2019**, *151*, 151102.
- [63] S. Mandal, V. Thakkur, N. N. Nair, *J. Chem. Theory Comput.* **2021**, *17*, 2244.
- [64] S. Mandal, N. N. Nair, *J. Comput. Chem.* **2020**, *41*, 1790.
- [65] S. Mandal, R. Kar, T. Klöföf, B. Meyer, N. N. Nair, *J. Comput. Chem.* **2022**, *43*, 588.
- [66] R. Seidel, M. Faubel, B. Winter, J. Blumberger, *J. Am. Chem. Soc.* **2009**, *131*, 16127.



- [67] J. Moens, R. Seidel, P. Geerlings, M. Faubel, B. Winter, J. Blumberger, *J. Phys. Chem. B* **2010**, *114*, 9173.
- [68] R. Ayala, M. Sprik, *J. Phys. Chem. B* **2008**, *112*, 257.
- [69] R. Ayala, M. Sprik, *J. Chem. Theory Comput.* **2006**, *2*, 1403.
- [70] M. Kılıç, B. Ensing, *J. Phys. Chem. B* **2019**, *123*, 9751.
- [71] M. Kılıç, B. Ensing, *J. Chem. Theory Comput.* **2013**, *9*, 3889.
- [72] A. Tiwari, B. Ensing, *Faraday Discuss.* **2016**, *195*, 291.
- [73] K. M. Rosso, J. R. Rustad, *J. Phys. Chem. A* **2000**, *104*, 6718.
- [74] W. W. Parson, *J. Phys. Chem. B* **2021**, *125*, 7940.
- [75] J. VandeVondele, R. Ayala, M. Sulpizi, M. Sprik, *J. Electroanal. Chem.* **2007**, *607*, 113.
- [76] Y. Tateyama, J. Blumberger, M. Sprik, I. Tavernelli, *J. Chem. Phys.* **2005**, *122*, 234505.
- [77] Y. Tateyama, J. Blumberger, T. Ohno, M. Sprik, *J. Chem. Phys.* **2007**, *126*, 204506.
- [78] M. Tachiya, *J. Phys. Chem.* **1989**, *93*, 7050.
- [79] X. Wu, A. Selloni, R. Car, *Phys. Rev. B* **2009**, *79*, 085102.
- [80] A. Damle, L. Lin, L. Ying, *J. Chem. Theory Comput.* **2015**, *11*, 1463.
- [81] T. D. Kühne, M. Krack, F. R. Mohamed, M. Parrinello, *Phys. Rev. Lett.* **2007**, *98*, 066401.
- [82] Copyright 2000-2021 jointly by IBM Corp. and by Max Planck Institute, Stuttgart., *CPMD, version 4.3* **2021**, <http://www.cpmd.org> (accessed on Oct 18, 2021).
- [83] T. Klöffel, G. Mathias, B. Meyer, *Comput. Phys. Commun.* **2021**, *260*, 107745.
- [84] A. D. Becke, *Phys. Rev. A* **1988**, *38*, 3098.
- [85] C. Lee, W. Yang, R. G. Parr, *Phys. Rev. B* **1988**, *37*, 785.
- [86] N. Troullier, J. L. Martins, *Phys. Rev. B* **1991**, *43*, 1993.
- [87] S. G. Louie, S. Froyen, M. L. Cohen, *Phys. Rev. B* **1982**, *26*, 1738.
- [88] G. J. Martyna, M. L. Klein, M. Tuckerman, *J. Chem. Phys.* **1992**, *97*, 2635.
- [89] J. Kolafa, *J. Comput. Chem.* **2004**, *25*, 335.
- [90] S. Amira, D. Spångberg, V. Zelin, M. Probst, K. Hermansson, *J. Phys. Chem. B* **2005**, *109*, 14235.
- [91] S. Amira, D. Spångberg, M. Probst, K. Hermansson, *J. Phys. Chem. B* **2004**, *108*, 496.
- [92] T. Remsungnen, B. M. Rode, *J. Phys. Chem. A* **2003**, *107*, 2324.
- [93] D. Semrouni, W. C. Isley, C. Clavaguéra, J.-P. Dognon, C. J. Cramer, L. Gagliardi, *J. Chem. Theory Comput.* **2013**, *9*, 3062.
- [94] S. T. Moin, T. S. Hofer, A. B. Pribil, B. R. Randolph, B. M. Rode, *Inorg. Chem.* **2010**, *49*, 5101.
- [95] S. A. Bogatko, E. J. Bylaska, J. H. Weare, *J. Phys. Chem. A* **2010**, *114*, 2189.
- [96] T. Remsungnen, B. M. Rode, *Chem. Phys. Lett.* **2004**, *385*, 491.
- [97] O. Boukar, J. J. Fifen, M. Nsangou, H. Ghalila, J. Conradie, *New J. Chem.* **2021**, *45*, 10693.
- [98] X. L. Lei, B. C. Pan, *J. Clust. Sci* **2012**, *23*, 311.
- [99] T. S. Hofer, H. T. Tran, C. F. Schwenk, B. M. Rode, *J. Comput. Chem* **2004**, *25*, 211.
- [100] H. Ohtaki, T. Radnai, *Chem. Rev.* **1993**, *93*, 1157.
- [101] B. S. Brunschwig, C. Creutz, D. H. Macartney, T.-K. Sham, N. Sutin, *Faraday Discuss. Chem. Soc.* **1982**, *74*, 113.
- [102] E. Kálmán, T. Radnai, G. Pálkás, F. Hajdu, A. Vértes, *Electrochim. Acta* **1988**, *33*, 1223.
- [103] M. Magini, T. Radnai, *J. Chem. Phys.* **1979**, *71*, 4255.
- [104] J. Cheng, M. Sulpizi, M. Sprik, *J. Chem. Phys.* **2009**, *131*, 154504.
- [105] J. Blumberger, G. Lamoureux, *Mol. Phys.* **2008**, *106*, 1597.
- [106] D. Lide, *CRC Handbook of Chemistry and Physics, Sec. 3: Physical Constants of Organic Compounds, 89th ed.*, CRC Press, Boca Raton, Florida **2008**.
- [107] W. M. Haynes, D. R. Lide, T. J. Bruno, *CRC Handbook of Chemistry and Physics, 96th ed.*, CRC Press, Boca Raton, Florida **2015**.